TWIN-BASED TOUGHENING MECHANISMS IN *PINNA NOBILIS* SHELL

Kinga Nalepka[1*], Katarzyna Berent[2*] Antonio G. Checa[3], Tomasz Machniewicz[1], Adrian J. Harris[4], Paweł Nalepka[1], Martyna Strąg[5], Łukasz Maj[5], Aleksandra Szkudlarek[2], Magdalena Bieda[5], and Krzysztof Sztwiertnia[5]

[1] Faculty of Mechanical Engineering and Robotics, AGH University of Science and Technology, Krakow, Poland
[2] Academic Centre for Materials and Nanotechnology, AGH University of Science and Technology, Krakow, Poland,
[3] Department of Stratigraphy and Palaeontology, University of Granada, Granada, Spain, and Andalusian Institute of Earth Sciences, CSIC-University of Granada, Armilla, Spain,
[4] Micro Materials Ltd., Willow House, Ellice Way, Yale Business Village, Wrexham LL13 7YL, UK
[5] Institute of Metallurgy and Materials Science, Polish Academy of Sciences, Krakow, Poland

Abstract

The shell structure of the *Pinna nobilis* species constitutes a model for others formed by bivalves of the Ostreida order. The outer part is built of monocrystalline columns whose axes remain parallel to the calcite *c*-axis. The present work reveals a new microstructure induced by mantle damage in the early stage of growth. The calcite *c*-axes, oriented perpendicularly to the strongly rough outer surface, deviate significantly from the shell thickness direction. The inclination angle is maintained up to the nacre layer. The transfer is made by the monocrystalline prisms which initially run along the *c*-axis and then deflect taking the thickness direction. They form coherent systems with low-energy twin boundaries. The uncovered twin relationships significantly improve the mechanical properties, as demonstrated using the nano-indentation and impact tests. Moreover, compression tests were performed, which confirms that the untypical structure exhibits a unique combination of high fracture toughness and strength.

1. Introduction

Bivalve shells are hierarchically complex biocomposites consisting of calcium carbonate with different polymorphs (calcite or aragonite) and an organic matrix [1]. The outer skeleton has been improved over millions of years of evolution to provide effective protection against predators. As a

* Corresponding author.
E-mail address: knalepka@agh.edu.pl (K. Nalepka)
kberent@agh.edu.pl (K. Berent)

result, the structures formed are lightweight and exhibit outstanding mechanical properties compared to materials from which they are built. Thus, the protective armors are an excellent source of inspiration for the formation of biomimetic engineering materials with an equally unique combination of high strength and fracture toughness [2 - 5]. Reproducing the shell's microstructure requires in-depth knowledge of it as well as identification of the mechanical properties of the components [6, 7]. The present work is part of the search for engineering materials inspired by nature. The subject of the study is a shell of the *Pinna nobilis* species with an unusual morphology due to the repair of an extensive injury occurred in an initial growth stage. Widespread observations indicate that the self-healing process generates a secondary structure with higher strength and fracture toughness than the primary one.

The Mediterranean pen shell *Pinna nobilis* Linnaeus, 1758 (superfamily Pinnoidea, Order Ostreida) is a large bivalve species that lives with its anterior end buried within the sediment (semi-infaunal), and attached by the byssus to clasts or shells within the sediment. It inhabits seagrass meadows and is presently an endangered and protected species. The shell is made of two layers with different microstructures. The outer layer has a columnar calcite prismatic (CCP) microstructure: large polygonal prisms elongated perpendicular to the outer shell surface, surrounded by organic sheaths. The inner shell layer is made of nacre and extends for less than half the anteroposterior diameter (e.g. [1]). This microstructural distribution is typical of the order Ostreida, except for the superfamily Ostreoidea. The two layers perform different functions. The thick periprismatic organic membranes make the outer prismatic layer particularly flexible [8]. When the two valves abut, shell closing is achieved by flexible deformation of the wide prismatic margins, providing a tight sealing ([9-10]). The inner nacreous layer is relatively thin and constitutes the tough and relatively rigid part of the shell. The prisms of *Pinna nobilis* may reach lengths of up to several mm, particularly in large specimens. From the crystallographic viewpoint, each prismatic unit is a single crystal (e.g. [1, 10-13]), with very low misorientation values ([14-17]), i.e., very similar to inorganic calcite crystals. The *c* axes of prisms remain parallel to their long axes [14, 18]. This is unlike other related bivalves, such as the pterioid *Pinctada margaritifera*, in which prisms display high orientation instabilities, which makes them break progressively into new crystalline domains [14].

The CCP layers of bivalves have been widely studied [19-25]. However, their mechanical properties have received little attention, particularly, when compared to nacre [26-29] and crossed-lamellar microstructures [30]. Strąg et al. [31] reported values of 460 MPa and 3.86 GPa for compressive strength and nanohardness of the calcitic layer of *Pinctada margaritifera*, respectively. Kunitake et al. [32] showed that the hardness of *Atrina rigida* CCP layer varies with the rotation of the indenter tip around the normal to the loaded *c* plane, i.e. with the azimuthal angle. Accordingly, the range of values obtained was 3.47–4.19 GPa at a penetration depth of 170 nm. A similar dependence was found by Böhm et al. [33] in *Pinna nobilis*: 3.89–4.86 GPa at a variable indentation depth 100–250 nm.

The aim of this study is to accurately identify the CCP microstructure of *P. nobilis* and link it with the mechanical properties of the constituent elements as well as with the response to the load of a representative shell volume. Investigations using the electron backscatter diffraction (EBSD) method have revealed new prism orientations, which play a key role in transferring the external load. This was demonstrated through theoretical analysis and then confirmed by the identification of mechanical properties at the local and global levels in the nano-indentation, nano-impact and compression tests.

2. Microstructure identification

The studied shell has a morphology unusual for the *P. nobilis* species. A clear division line running longitudinally on both valves is visible (Fig. 1a). The probable reason is the damage of the mantle at the initial stage of growth. As a result, two separate parts develop, and the shell acquired a bilobate appearance. Besides the division, the outer shell surface exhibits a significant roughness (Fig. 1b-e), which is related to the formation of thin calcitic ribs, produced by the pleated border of the mantle. The disturbed geometry entails untypical microstructure. In order to identify it, the in-depth EBSD investigations were carried out.

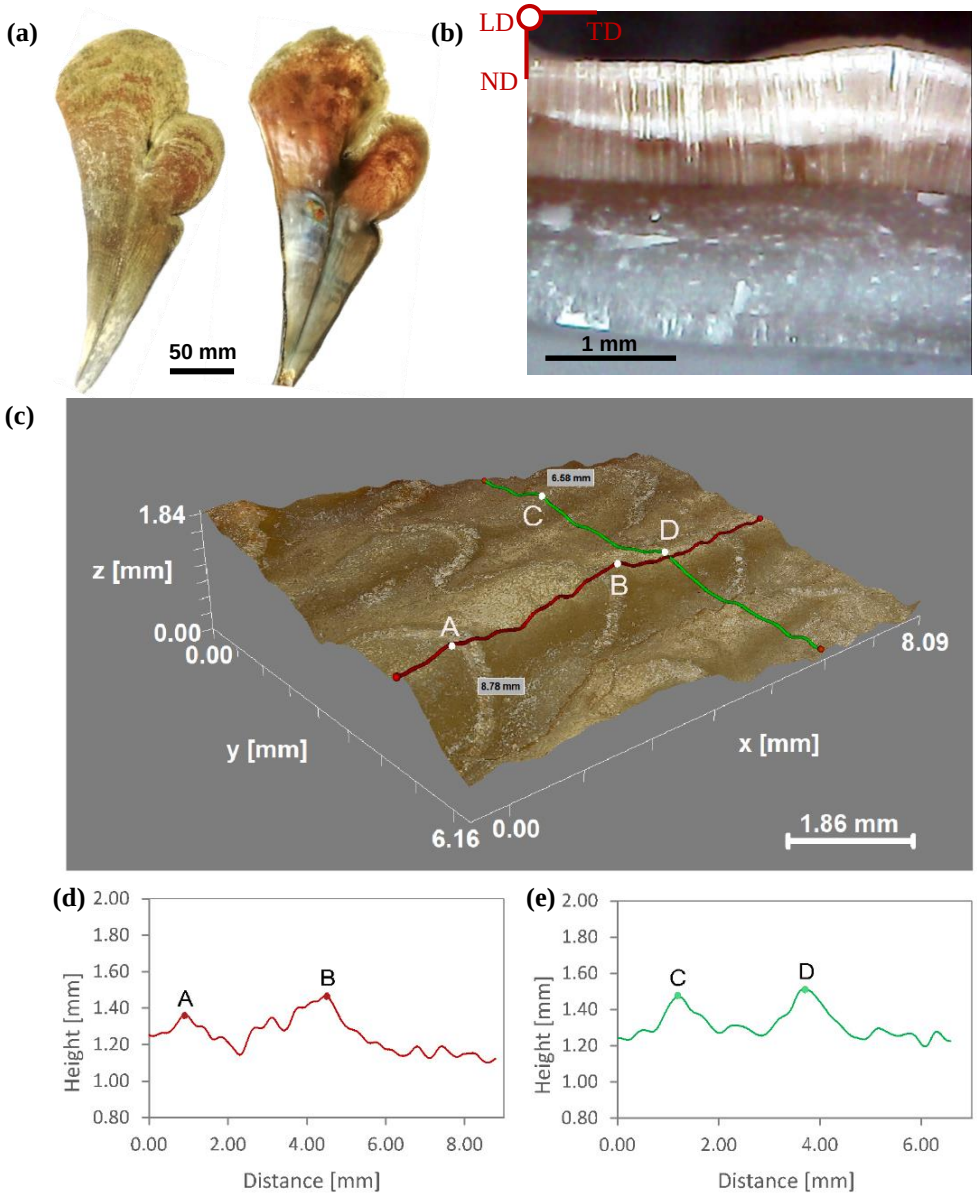

Fig. 1 Morphology of *Pinna nobilis* shell. (a) outer and inner view of the specimen showing the bilobate margin produced by shell repair. (b) cross-section of the shell determined by normal (ND) and transversal (TD) directions. (c) surface with roughness measured along (d) longitudinal (LD) and (e) transversal (TD) direction

The prisms, growing perpendicularly to the repaired outer surface, deviate from the normal direction (ND) determined by the shell thickness. As a result, in the outer layer, the directions of fast growth i.e. *c* axes of calcite crystals are mostly oblique (Fig. 2). With the shell development, growth lines become flatter and the orientation of the growth axes of prisms becomes more and more parallel to ND. This process leads to the deflection of prisms as well as to the elimination of those that exhibit a significant initial deviation from the normal direction (Fig. 2a). The ordered orientation of prisms does

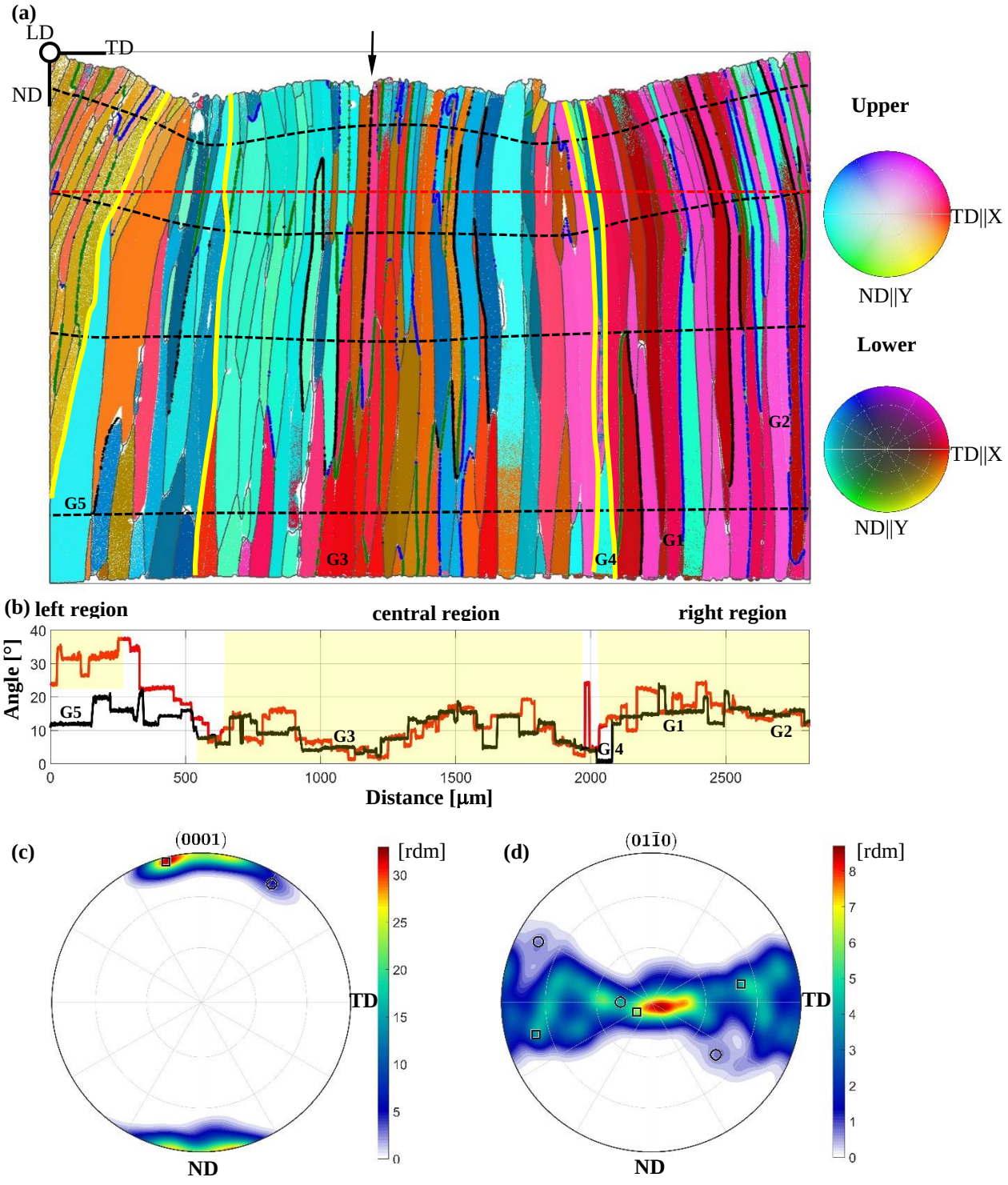

Fig. 2 Microstructure of representative cross-section. (a) Orientation in axis/angle colour coding. The regions with distinct microstructures are separated by yellow lines whereas the trace of a morphological symmetry plane is indicated by an arrow. The growth lines are denoted by black dashed lines, while boundaries with specific disorientations A, B, C are marked in green, blue and black (b) Angle of deviation of the *c* axis from ND depending on the position determined by the level of the second (red) and the last (black) growth line. (c), (d) Pole distribution function (PDF) for $\{0\ 0\ 0\ 1\}$ and $\{0\ 1\ \bar{1}\ 0\}$ planes together with the most frequent orientations in the left (circle) and right (square) region.

not mean that it is preserved by calcite grains. It turns out that during the growth of crystallites, the *c*

axes maintain their initial direction. As a result, incorrectly, obliquely initiated orientation becomes obligatory on the entire thickness of the shell. Thus, the island-shaped surface determines the structure of the entire protective armor. Analysis of the EBSD results reveals a clear division into three areas. The middle one is initiated by an island (a local shell elevation) with a small curvature, while the lateral ones begin with a greater slope. As a result, in the central region, the *c* axes of prisms are the most frequently tilted by a small angle of 12° relative to ND, and their initial orientation is maintained up to the nacre layer (Fig. 2b). The central area is flanked by fragments of islands with a larger curvature, particularly on the left. They initiate regions in which the *c* axes of grains most often orientate at an angle of 32° and 14° relative to ND, respectively (see Fig. 2c). The organization of both zones is similar. Initially formed grains with an oblique inclination tend to disappear, whereas their neighbors expand at their expense. In this way, crystallites with *c* axes significantly deviated from ND are eliminated while those which form a group with a similar orientation of *c* axes reach the nacre layer (G1, G2). Each prism constitutes a single calcite crystal. Even its sudden deflection causes only a slight change in the orientation of calcite - the difference remains within 2° (G2).

The orientation of grains is presented in the convention of axis/angle rotation with the use of a color code. The color determines the position of the axis according to the pole figures (Fig. 2a). The other variable - the angle of rotation is expressed by the color saturation. Thus, 0° and 90° correspond to gray and full saturation, respectively. Grains, typical for *Pinna nobilis*, with axis *c* || ND, are generated by means of an axis with red (e.g. G3) or blue pole (e.g. G4). Then the rotation by 90° moves the *c* axis to the ND position. A strong prism slope in the lateral areas prevents contact with the central region. The resulting gaps are filled by additional prisms. They enable a smooth transition between distinct regions by introducing a gradual rotation of the *c* axis towards ND (G5).

The question arises whether there is a preference in the mutual orientation of adjacent grains. The calculated Misorientation Distribution Function (MDF) shows that the crystallites rotate with respect to each other around the *c* axis, taking three preferential positions. They are determined by the following values of the rotation angle ω: 18° (A), 38° (B) and 60° (C) (Fig. 3a). High preference is usually due to the system's striving to the formation of low-energy boundaries. Hence, calculations were carried out which reveal how interfacial energy changes when adjacent calcite crystallites are rotated

around the *c* axis. Accurate determination of the quantity for the continuous rotation is virtually impossible due to the too high computational cost. Therefore, an approximated method developed by Gautam and Howe [34] is used. According to it, interfacial energy decreases with the increase of the total intensity *I* contained in the areas of overlapping the diffraction reflections from neighbouring crystallites. Thus, using the last quantity we can find disorientations, to which local energy minima correspond (see Sec. 6).

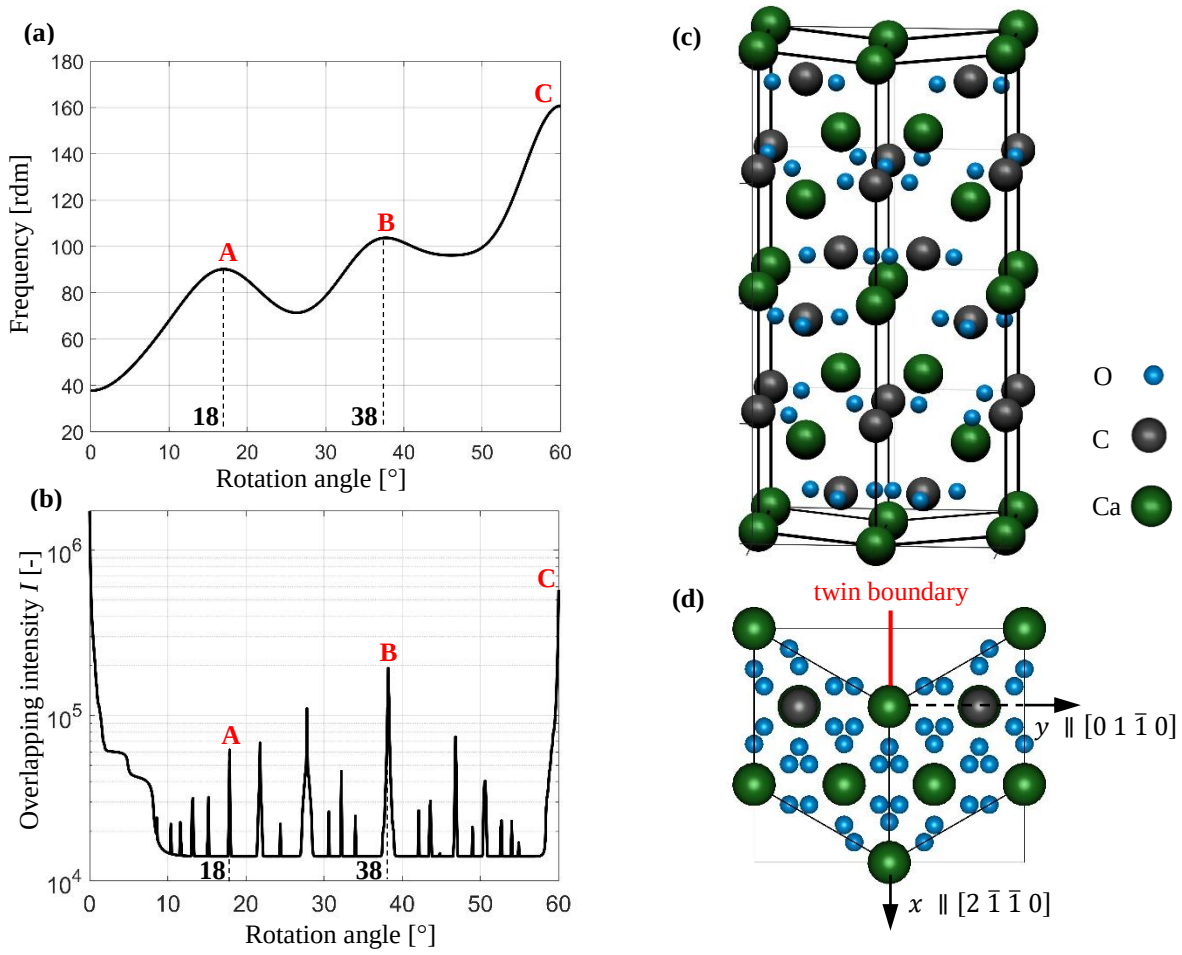

Fig. 3 Preference in the misorientation of grains. (a) Distribution of disorientation angle for rotation about *c* axis showing three preferred disorientations between calcite crystals of the cross-section (A, B, C) (b) Dependence of overlapping intensity *I* on the disorientation angle of rotation around the *c* axis. The local maxima determine low-energy disorientations. (c), (d) $(0\ 1\ \bar{1}\ 0)$ calcite twin.

The results clearly show that strictly defined low-energy boundaries, i.e. rotation angles, are preferred (Fig. 3b). Particularly important is the disorientation based on rotation around the *c* axis by 60°. Two symmetrically equivalent orientation relationships correspond to it. They constitute two twin boundaries formed by the reflection planes $(0\ 1\ \bar{1}\ 0)$ and $(0\ 0\ 0\ 1)$, respectively. The prismatic

structure, whose elements mostly run through the entire thickness of the shells, causes that the first of them mainly occurs. The twin boundary $(0\ 1\ \bar{1}\ 0)$ positioning perpendicular to the growth line, allows it to be curved (comp. Fig. 3c, d and Fig. 4a, b). As a result, grains separated by a morphological plane of symmetry form a coherent connection. Another example is the boundary running along the symmetry axis of the central region (indicated by the arrow in Fig. 2a). The other preferred disorientations are also generated by twin relationships but this time the mirror planes have higher indices $(1\ \bar{5}\ 4\ 0)$ and $(4\ 7\ \overline{11}\ 0)$ for 38° and 18°, respectively. These two uncovered twins are formed only in biogenic calcite. They define new, hitherto unknown orientation relations.

Something one could wonder is how twin relationships can exist when monocrystalline prisms are separated by thick organic membranes. Checa et al. [24] showed how new membranes are introduced very early during the growth of prisms in the CCP layers of several pterioids, thus dividing otherwise continuous crystalline domains. We can hypothesize that twins were formed in initial growth stages in *Pinna* and twinned crystals were later separated by membranes. Given the low misorientations recorded in Pinna prisms, crystals remained in twin relationship long after they were separated by membranes. The EBSD investigations performed for the representative fragment of the shell surface confirm that the slopes associated with island-like morphology lead to calcite prism inclination (Fig. 4). The *c* axes oriented perpendicular to the curved surface assume four preferential positions. It is revealed by the pole distribution function (PDF) whose four maxima show that *c* axes deviate from ND by 26°, 16°, 38°, and 36°, respectively (Fig. 4c). The identified orientations of *c* axes reflect the microstructure division into regions in which grains start to grow from differently sloping surfaces. The four zones formed are clearly depicted by means of axis/angle colour coding (Fig. 4b). Both calcite crystals situated along the ND, as well as those inclined rotate around their *c* axes, showing a tendency to locate the planes {0 1 -1 0} perpendicular to the longitudinal direction (Fig. 4d). Actually, the rotation is continuous, so there are not clear angular preferences (Fig. 4e). We can say, that in the initial growth stage the misorientation of prisms is largely random. With shell development, low-energy boundaries are continued and others tend to disappear. It is shown by the results obtained for the cross-section (Fig. 3a, b). The surface image captures the area of elongated grains, whose longer boundaries are determined by the directions of growth. At the place of strong curvature in the growth line, they deviate from each other. It is enabled

by the twin boundary that runs along the longitudinal direction (LD) (comp. Fig. 3d and Fig. 4a, b). In this way, the mirror symmetry between adjacent grains is combined with the symmetry of the entire area morphology.

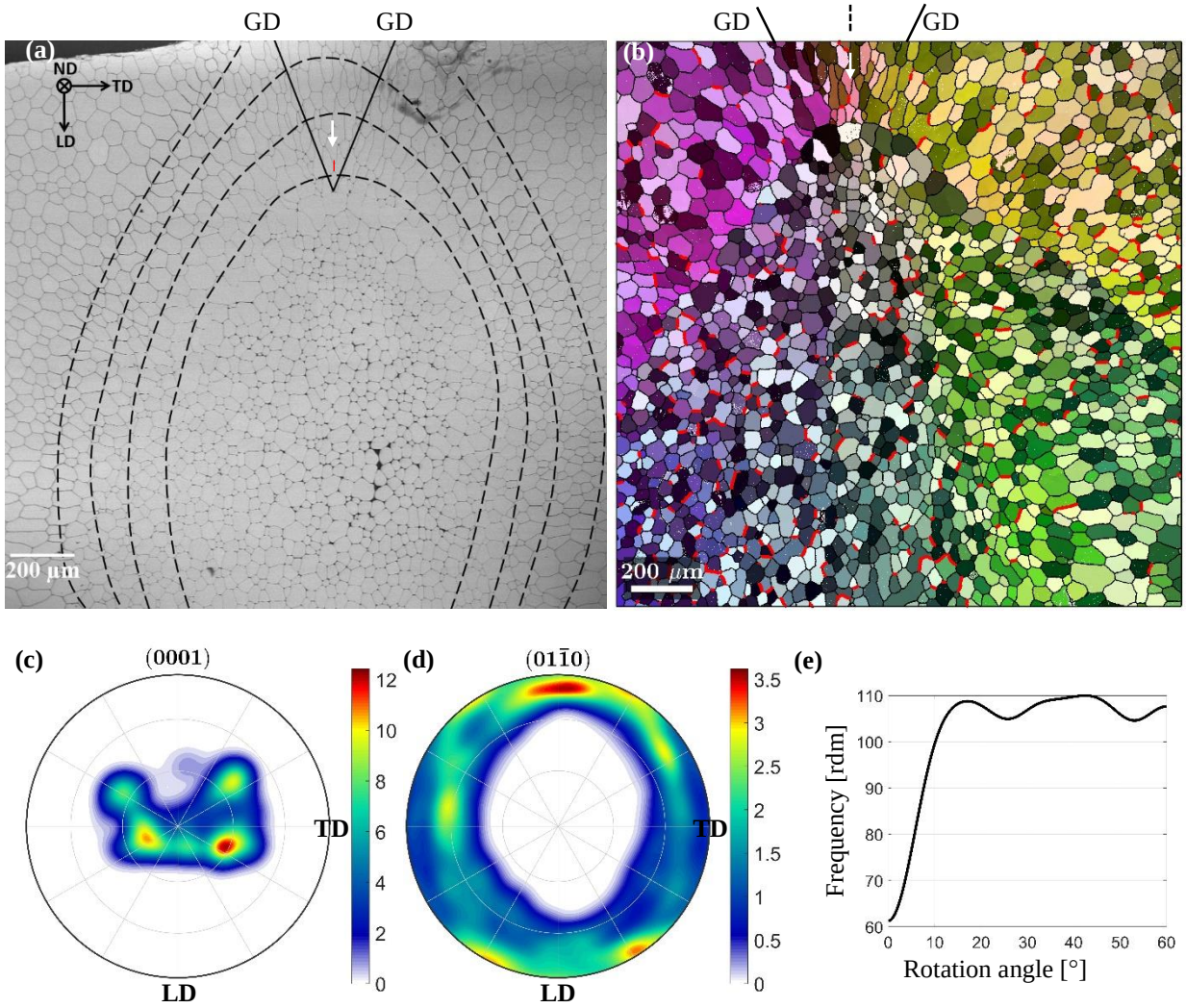

Fig. 4 Microstructure of the outer shell surface. (a) SEM image with growth lines denoted by black dashed lines. (b) Grain orientation in axis/angle colour coding. Twin boundaries $(0\,1\,\bar{1}\,0)$ are marked in red. One of them providing a smooth change in the growth direction (GD) is indicated by a white arrow. (c), (d) PDF for $\{0\,0\,0\,1\}$ and $\{0\,1\,\bar{1}\,0\}$ planes. (e) Distribution of disorientation angle for rotation about *c* axis.

The question arises how the unique microstructure affects the mechanical properties of the material. In order to solve the problem posed, research was carried out at different levels of the scale. In the first stage, static and dynamic nano-indentation of prisms with various orientations was performed. Then, we conducted static compression tests of cubic elements representing shell areas with strongly inclined *c* axes.

3. Nano-indentation tests

3.1. Theoretical analysis

Calcite anisotropy makes the prism orientation a key determinant of global mechanical properties. The arrangement of these basic structural units controls the activation and course of plastic deformations, brittle fracture processes as well as their mutual coupling.

Experiments carried out for the geological single calcite crystal have identified two basic mechanisms of glide r $\{0\,\bar{1}\,1\,4\}\langle 0\,2\,\bar{2}\,1\rangle^{\pm}$, f $\{\bar{1}\,0\,1\,2\}\langle 2\,\bar{2}\,0\,1\rangle^{\pm}$ and one of twinning e $\{\bar{1}\,0\,1\,8\}\langle 4\,0\,\bar{4}\,1\rangle^{+}$. At room temperature, despite the high pressure caused by indentation, not all slip systems are activated, but only three of six of each type: $r\,\langle 0\,2\,\bar{2}\,1\rangle^{-}$, $f\,\langle 2\,\bar{2}\,0\,1\rangle^{-}$. Of course, it depends on the resolved shear stress operating in a given slip system. The lowest critical value of 110 MPa was identified for the r planes [35]. Hence $r\,\langle 0\,2\,\bar{2}\,1\rangle^{-}$ slips play a key role in the plastic deformation of calcite grains. The resolved shear stress can be determined by the Schmid factor S according to the relationship: $\tau = \sigma_0 S = \sigma_0 \cos\varphi \cos\lambda$, where σ_0 is normal stress on the indented surface, while φ and λ are angles between the loading direction and the normal of a slip plane $\hat{\boldsymbol{n}}$ or a slip direction $\hat{\boldsymbol{s}}$, respectively. The Schmid factor depends on orientation of a grain and the slip system which is activated inside it. If we assume an initial reference system with the z axis parallel to the loading direction (see Fig. 5a) and a final one determined by the system of a rotated crystal $\hat{\boldsymbol{x}}_{\boldsymbol{c}} \parallel [2\,\bar{1}\,\bar{1}\,0], \hat{\boldsymbol{y}}_{\boldsymbol{c}} \parallel [0\,1\,\bar{1}\,0], \hat{\boldsymbol{z}}_{\boldsymbol{c}} \parallel [0\,0\,0\,1]$ (Fig. 5), then the considered coefficient can be expressed by Euler angles and coordinates of unit vectors of the analyzed slip system $\hat{\boldsymbol{n}}$ and $\hat{\boldsymbol{s}}$. As a result, we obtain the following formula:

$$S = \left(n_x \sin\varphi_2 \sin\Phi + n_y \cos\varphi_2 \sin\Phi + n_z \cos\Phi\right)\left(s_x \sin\varphi_2 \sin\Phi + s_y \cos\varphi_2 \sin\Phi + s_z \cos\Phi\right) \quad (1)$$

The relation is depicted for those slip systems, that give the highest values of the Schmid factor in the case of indented grains (Fig. 6a-c). A positive sign of the quantity means agreement between the signs of the applied normal stress and the resulting slip in the considered system. Interpretation becomes easier if we take into account positive slip systems. Then, a positive S factor means that during unloading a positive slip arises, while at the loading stage a negative slip is generated.

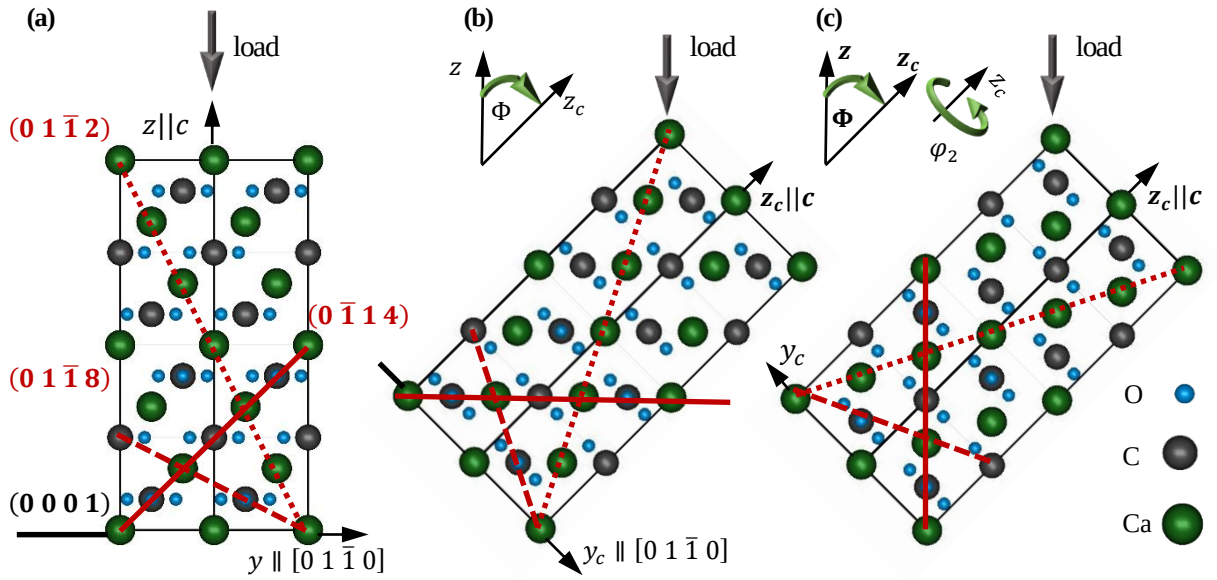

Fig. 5 Typical and inclined grains. (a) Two calcite elementary cells at the initial position (b) and after rotation by an angle $\Phi = -45°$, which is equivalent to $\Phi = 45°, \varphi_2 = 60$ in asymmetric domain of the orientation space. (c) Twin of the crystal (b), $\Phi = -45°, \varphi_2 = 180°$, which is equivalent to $\Phi = 45°, \varphi_2 = 0°$ in asymmetric domain. The planes for plastic and brittle deformation are also depicted.

Ionic bonding of calcite makes it prone to brittle fracture. The key cleavage planes are $\{0\ \bar{1}\ 1\ 4\}$ Separating a unit area of such a surface from the bulk crystal requires relatively little work, i.e. surface energy γ_{CP}. Subsequent cleavage planes with higher surface energy are $\{\bar{1}\ 1\ 0\ \bar{8}\}$ and $\{0\ 0\ 0\ 1\}$. The classification presented is based on the results obtained by Bruno *et al.* [36] using the molecular dynamics method. According to their calculations, the relaxed surface energy at 0 K for individual planes is 0.534, 0.702 and 0.711 J/m^2, respectively. Fracture along a given plane requires appropriate normal stresses. They arise during nano-indentations at the unloading stage. Their value can be calculated on the basis of simple geometrical relationships if we assume that there is a one-dimensional stress state σ_0 under the indenter: $\sigma = \sigma_0 cos^2\varphi = \sigma_0 C$. Thus, the amount of tensile stress on a given plane is determined by the cleavage factor *C*. Its value depends on coordinates of a unit vector normal to the plane and Euler angles that orientate an intended grain. This is expressed by the following formula:

$$C = \left(n_x \sin\varphi_2 \sin\Phi + n_y \cos\varphi_2 \sin\Phi + n_z \cos\Phi\right)^2 \quad (2)$$

The relation is illustrated for three planes representing the mentioned families. The chosen planes generate the highest values of the factor in the case of intended grains (Fig. 6d-f).

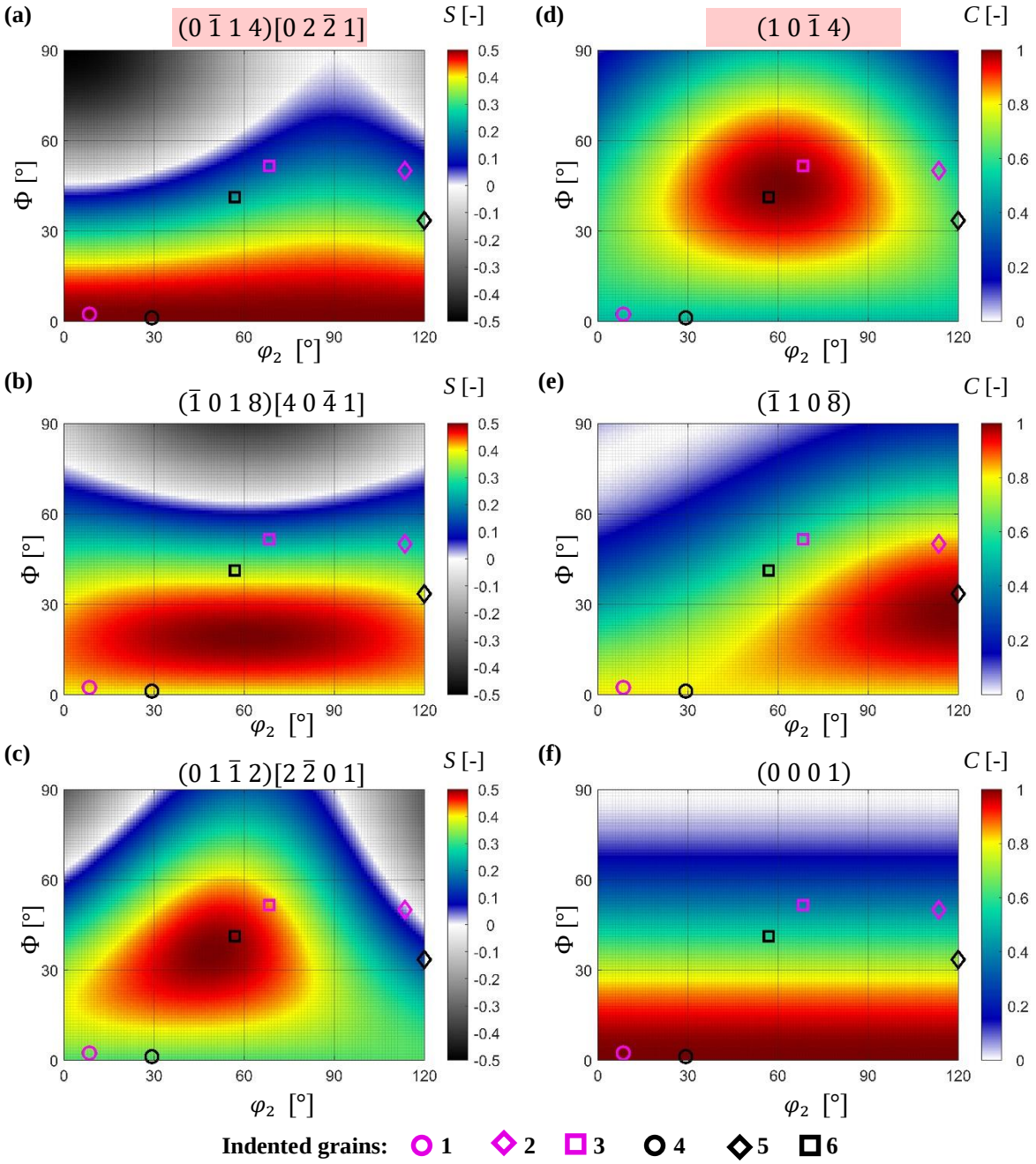

Fig. 6 Schmid factor *S* and cleavage factor *C* for representative slip systems and fracture planes as functions of the crystal orientation determined by Euler angles. The relationships are presented for those slip systems and cleavage planes at which the coefficients achieve the highest values in indented grains 1–6.

Prisms typical of the *Pinna nobilis* species with the *c* axes running along the shell's thickness (ND) (Fig. 5a) are not the best mechanical solution. Then, regardless of the rotation of the grain around the *c* axis, a maximal resolved shear stress equal to half the compressive stress applied to the outer surface is generated in the $(0\ \bar{1}\ 1\ 4)[0\ 2\ \bar{2}\ 1]^{-}$ system (Fig. 6a). Thus, in a given orientation of the prism slips can be activated in three planes $\{0\ \bar{1}\ 1\ 4\}$ simultaneously. Similarly, basic twin systems

$\{\bar{1}\ 0\ 1\ 8\}\langle 4\ 0\ \bar{4}\ 1\rangle^{+}$. achieve a high Schmid factor exceeding 0.4 (Fig. 6b). They are activated during unloading. As a result, grains typical of *Pinna nobilis* undergo intensive plastic deformations. Moreover, there is a possibility of fracture along the $\{0\ 0\ 0\ 1\}$ plane because during unloading tensile stresses are perpendicular to it (Fig. 6f).

Geometric analysis of plastic processes shows that the inclination of grains significantly improves their mechanical properties. Due to deviation of *c* axis from the outer surface normal, the systems of easy slips are so-oriented that the formation of shear stresses necessary to induce permanent deformations is difficult. As the angle Φ increases, the factor *S* of the slip family $\{0\ \bar{1}\ 1\ 4\}\langle 0\ 2\ \bar{2}\ 1\rangle$ decreases (Fig. 6a). Thus, during loading the key glide mechanism *r* $\langle 0\ 2\ \bar{2}\ 1\rangle^{-}$ is confined. At the appropriately high stress a single system $(0\ 1\ \bar{1}\ 2)[2\ \bar{2}\ 0\ 1]^{-}$ is activated. Initially, it is constrained to a small group of grains with orientations near the (49°, 35°) point which constitutes a maximum of Schmid factor (Fig. 6c). It is worth noting that, at the same time, in other systems of this family, the *S* coefficient does not exceed 0.13. At the unloading stage, the glide mechanism *r* $\langle 0\ 2\ \bar{2}\ 1\rangle^{-}$ is not activated at all. Instead, in single systems $(\bar{1}\ 0\ 1\ 8)[4\ 0\ \bar{4}\ 1]^{+}$ and $(\bar{1}\ 1\ 0\ \bar{2})[0\ 2\ \bar{2}\ 1]^{-}$, twinning and slipping occur respectively. Starting the last process is identified by the Schmid factor, which at point (71°, 35°) reaches the minimal value -0.5.

Thus, with a relatively low external load, the glide processes inside typical grains are activated. When the prisms deviate from ND above 30°, the initiation of slips requires the application of higher normal stresses to the outer surface. Then confined plastic deformations will occur in the systems *r* $\langle 0\ 2\ \bar{2}\ 1\rangle^{-}$, and in grains with a specific orientation will continue in a single system $(0\ 1\ \bar{1}\ 2)[2\ \bar{2}\ 0\ 1]^{-}$. Thus, the degree of permanent deformation is lower. In the case of engineering materials, an increase in strength is associated with a decrease in fracture toughness. This relationship also affects the *Pinna nobilis* protective armor, but is limited to a small group of grains with specific orientations determined by Euler's angles from the vicinity of the (60°, 45°) point (Fig 6d). Then the plane of easy cleavage $(1\ 0\ \bar{1}\ 4)$ is located perpendicular to the normal force acting on the outer surface (see Fig. 5b). Hence, during unloading, an extensive crack will form. Other grains tend to split along planes $\{\bar{1}\ 1\ 0\ \bar{8}\}, \{0\ 0\ 0\ 1\}$. Then separation requires higher energy. Hence, the fracture process is initiated at a

higher load and is often combined with plastic deformation, which limits the crack growth. To sum up, the anisotropy of calcite crystal makes the inclined prisms show higher strength and fracture toughness in comparison to those with *c* axes parallel to ND. An exception is a small group in which planes $\{1\,0\,\bar{1}\,4\}$ orient perpendicular to ND. Nevertheless, the twin boundary $(0\,1\,\bar{1}\,0)$ transforms the grains into the adjacent ones which show significantly higher strength and toughness (Fig. 5c).

3.2. Experimental results

The regularities revealed in the theoretical analysis are mapped by the relation that combines the values of the mechanical property measured for representative grains in the nano-indentation test. Two groups were studied, each of which consists of three grains. The first prism preserves the *c* axis parallel to ND, the second one shows a strong inclination, while the other due to the specific tilting has a plane $\{1\,0\,\bar{1}\,4\}$ oriented perpendicular to ND with an accuracy of 10°. Schmid and cleavage factors for individual grains are presented in previously prepared distributions (Fig. 6). The first prism exhibits the lowest hardness, the second one, the highest, and the third one is characterized by an intermediate value (Tab. 1). The obtained maps show that the response of the second grain is largely uniform, while that of the first one is varied. A large part of prism 1 exhibits a hardness at a low level of 3.0 GPa (Fig. 7c, d). The higher average value results from locally occurring harder areas. Research conducted on biogenic calcite shows that one of the sources of improving mechanical properties are structural defects [32].

Table 1 Mechanical properties of the shell's grains

Grain	Hardness [GPa]	Reduced elastic modulus [GPa]
1	3.26 ± 0.38	66.8 ± 4.8
2	3.55 ± 0.34	66.4 ± 4.2
3	3.44 ± 0.34	75.1 ± 5.3

Experimental results confirm theoretical predictions. Grains typical for *Pinna nobilis* easily undergo plastic deformation. Inclination significantly hinders these processes, which induces the hardness increase.

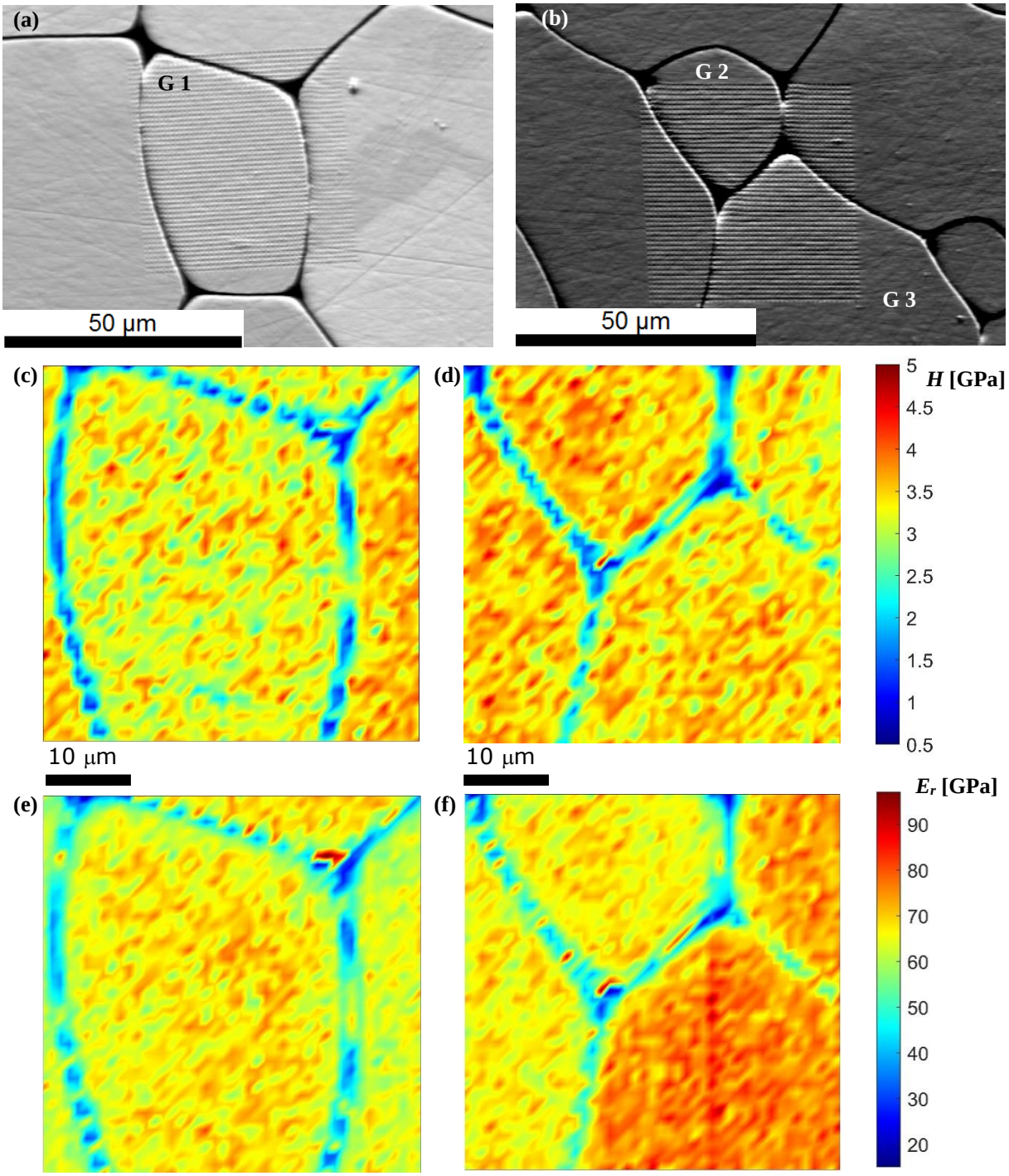

Fig. 7 Nanoindentation results on individual grains. (a), (b) SEM images of the indented areas. (c), (d) hardness distribution. (e), (f) reduced elastic modulus distribution.

Interestingly, the values of elastic modulus are ordered in a different way. The grain with the medium hardness attains the highest stiffness 75.1 GPa. The reason is the densely packed plane which is located almost perpendicular to the load direction. This grain forms a twin relationship with the adjacent one 2. The rotation that occurs then causes the plane $(1\ 0\ \bar{1}\ 4)$ to be almost vertical, i.e. parallel to ND. As a result, the mechanical response is determined by a random plane with high indices. Its rare

packing makes the elastic modulus the lowest. Orientations of prisms 3 and 2 are similar to those shown in Fig. 5. The first of these crystals exhibits the maximal cleavage factor for the key plane $(1\,0\,\bar{1}\,4)$. The other one, due to the twin relationship, reduces this coefficient to 0.

Additional information on how the orientation of the grains controls the mechanical properties is provided by the second group of grains subjected to the impact test. Most cracks are formed in prism 4, typical for *Pinna nobilis* shells (Fig. 8a). They develop in a radial direction from the corners of the

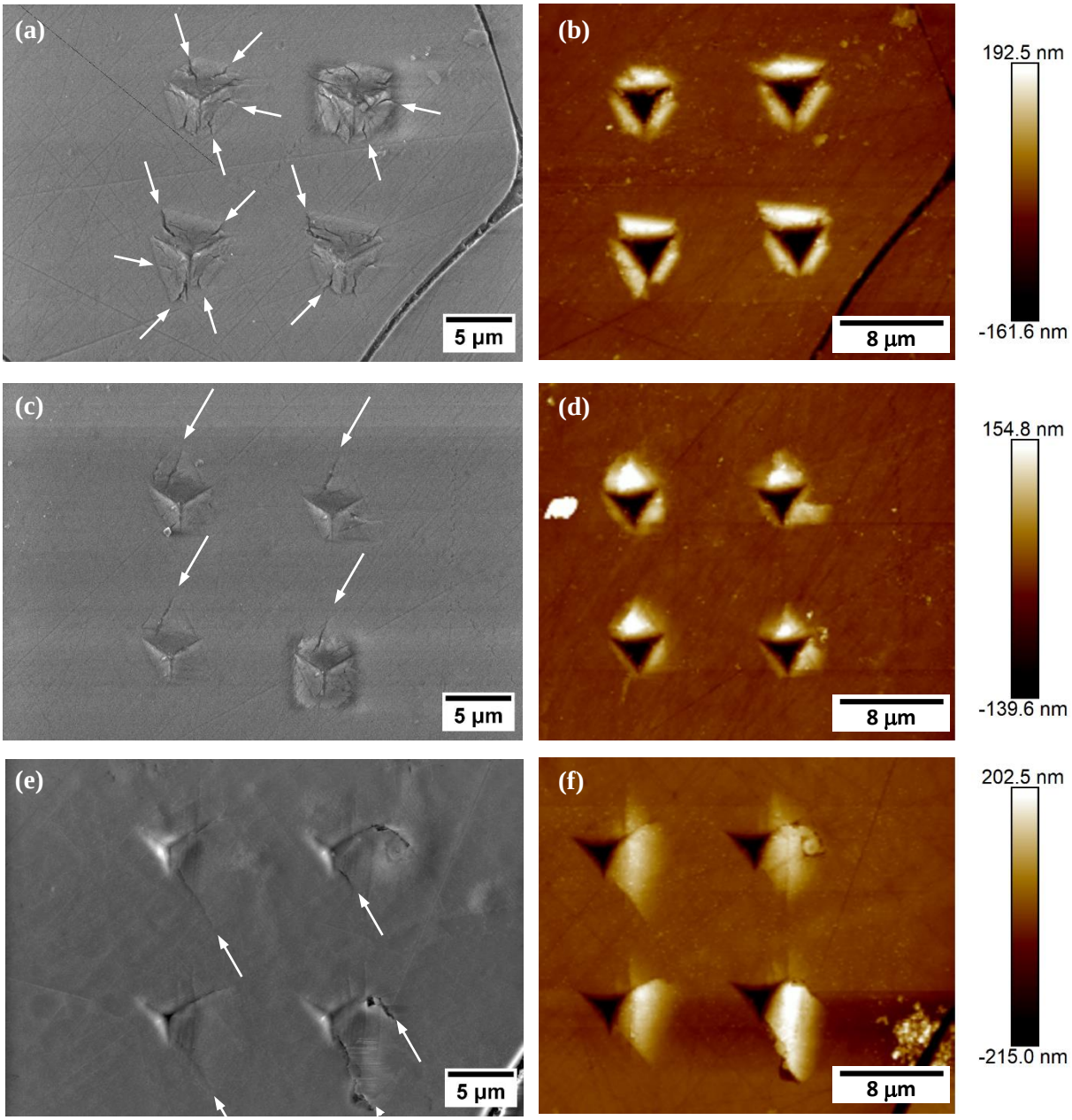

Fig. 8 Scanning electron microscopy (SEM) and atomic force microscopy (AFM) images of impressions in grains with different orientations. (a) (b) prism 4 with *c* || ND, (c) (d) inclined prism 5, (e) (f) inclined prism 6 with the plane $(1\,0\,\bar{1}\,4)$ nearly perpendicular to ND. The traces of planes $\{1\,0\,\bar{1}\,4\}$ are indicated by arrows.

impression or along the traces of planes {1 0 -1 4}. The reason is significant plastic deformation caused at the loading stage. As in the case of the indentation of synthetic ceramics [37], the zone of plastic deformation located below the impression becomes a source of cracks which propagate to the external surface. According to theoretical analysis, a grain with axis *c* || ND undergoes the strongest plastic deformation. This gives rise to a dense crack system. They combine to form surfaces along which portions of material adjacent to the indents' edges undergo separation. The inclined grain represented by prism 5 behaves completely differently. Individual cracks are consistently running along the traces of the $(0\ \bar{1}\ 1\ 4)$ plane deviated by an angle of 38° from the surface (Fig. 8c). Thus, decohesion occurs at a lower depth, and in many cases is only partial. The atomic force microscopy (AFM) measurements show that the depths and areas of the impressions as well as the heights of the material pileups are smaller compared to grain 4 (comp. Fig. 8d and Fig. 8b). The visible reduction of plastic deformation as well as limitation of fracture processes is induced by the prism inclination. Higher strength and fracture toughness means that absorption of the impact energy is much lower than in the case of grain 4. This is indicated by greater distance to which the indenter is bounced from the sample back. It amounts 4000 nm, whereas for grain 4 it is 3800 nm. A small group of oblique grains shows reduced fracture toughness. It is represented by prism 6, which is illustrated in Fig. 6d. Then, during unloading, tensile stresses generate lateral cracks along the easy cleavage plane $(1\ 0\ \bar{1}\ 4)$ almost perpendicular to ND. As a result, the material is chipped, which partly occurs along the plane $(1\ \bar{1}\ 0\ \bar{4})$ deviated by the large angle of 71° from the surface (Fig. 8e, f). Both the depths of impressions and the volumes of material detached from the bulk are the largest among the grains tested. Extensive damage entails significant absorption of impact energy, resulting in a shorter distance of the indenter bounce - 3600 nm.

4. Compression tests

Besides the identification of mechanical properties at the nano- and microscopic levels, the response at the macroscopic level was also examined. The compression test was carried out for 6 samples cut from the rib areas at the places of outgrowths (see Fig. 4b) where the prisms strongly deviate from ND. The results in the form of the stress-strain diagram together with the compressive strengths (σ_c) determined for the individual shell specimens are presented in Fig. 9.

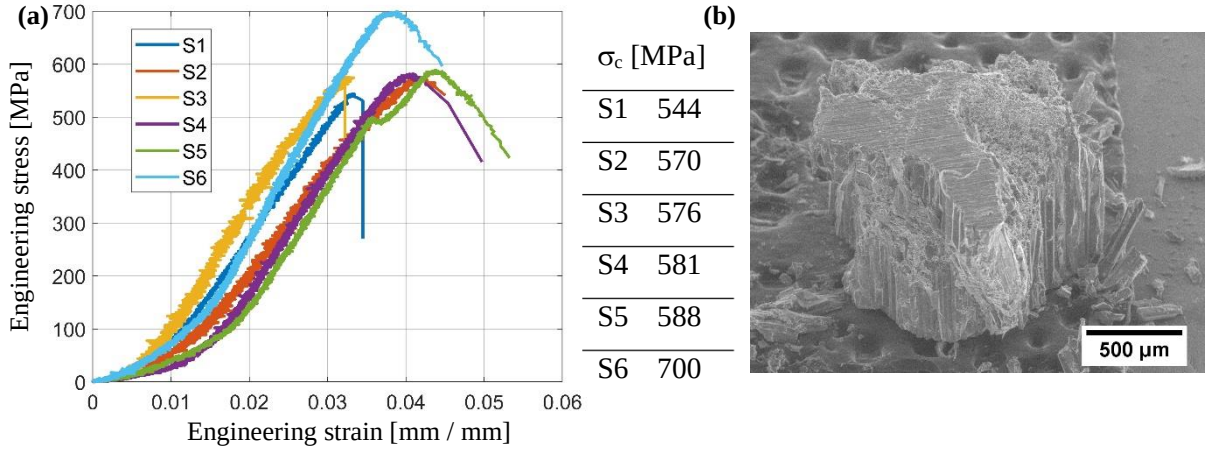

Fig. 9 Response of *Pinna nobilis* shell specimens to compression. (a) stress – strain curves together with compressive strength. (b) SEM image of specimen no. 5 after compression.

The values obtained are remarkably high considering the mechanical properties of the materials the shell is made of. Compressive strength up to 700 MPa results from the unique structure which is a weave of strong and weak units. This gives a great ability to dissipate energy, as well as enables blocking and delocalization of the fracture process. As a result, the loss of load capacity occurs at high stresses, when a significant part of the structure, or even the entire one is destroyed. Examples of such mechanical responses are samples 5 and 6, respectively.

5. Conclusions

The subject of the study is a non-typical shell of the *Pinna nobilis* species. Mantle damage, possibly due to a predator attack, at an early stage of growth caused retraction of the shell margin at the point of injury, with the subsequent formation of a bilobate margin in both valves. The disturbance in the lie of the external surface induces significant roughness. The structure initiated by the process of self-healing shows a different arrangement from the naturally occurring one. Basic units (calcite prisms) starting the growth, orientate obliquely to the thickness direction. Angles between the *c* axes of calcite grains and ND are considerable and often exceed 30°. With development, the structure is being ordered and the prisms reach the nacre layer perpendicularly. Despite this, the grain crystallographic *c* axes preserve their initial oblique orientation. The EBSD investigations reveal that misorientation of grains is not random. Most often they rotate relative to each other around the *c* axis by 18°, 38° and 60°. In order to uncover the reason of the observed strong preference, it was calculated how the interface energy changes

during the continuous rotation of one grain relative to the adjacent one. The results obtained show that basic, structural units – prisms are combined along low-energy boundaries. The preferred disorientations constitute twin relationships. Thanks to them, a dominant *c* axis orientation is formed at the outer surface of the shell and then it is transferred deeper up to the nacre layer. The twin boundary $(0\ 1\ \bar{1}\ 0)$ generates the largest rotation around the *c*-axis - 60°. Thus, it is often located along the symmetry axis of the shell rib enabling strong curvature of the growth line while maintaining coherency of the areas on the left and right. The structure consisting of calcite grains with *c* axes significantly deviated from the normal to the external surface shows unique mechanical properties. This was explained by the determined distributions of the Schmid and cleavage factors. The processes of permanent deformation and brittle fracture mainly proceed along the planes of easy slip and easy cleavage. In calcite, the role is played by one family $\{1\ 0\ \bar{1}\ 4\}$. If the angle of inclination exceeds 30°, the orientation of these planes hinders both plastic slips at the loading stage and propagation of cracks during unloading. An exception is a small group of grains in which one of the planes $\{1\ 0\ \bar{1}\ 4\}$ is located perpendicularly to ND. Nevertheless, the specific microstructure enables blocking the extensive crack which arises then. A perfect tool is the twin boundary $(0\ 1\ \bar{1}\ 0)$, which transforms the weak grain into a strong counterpart. Theoretical results are confirmed by the nano-indentation test. Typical grains for *Pinna nobilis* with a *c* axis parallel to ND undergo advanced plastic deformations, which leads to the lowest hardness. Inclination significantly increases its value. Similarly, the impact test induces intensive fracture of the typical grains. On the surface, numerous cracks running in the radial direction and along the traces of planes $\{1\ 0\ \bar{1}\ 4\}$ are formed. The grain inclination significantly confines the fracture process. Only single cracks are observed on the external surface. The energy dissipated then is small, which is confirmed by a significantly greater bouncing distance of the indenter than in the case of typical grains. Samples representing shell areas with strongly tilted *c* axes were subjected to a compression test. Their strength is surprisingly high - it reaches 700 MPa. The excellent mechanical properties of the biogenic material result from the weave of strong and weak structural units. The former provides load transfer, while the latter constitute zones of controlled energy dissipation, which is necessary to reduce brittle fracture processes.

6. Materials and Methods

Microstructure investigations. *Pinna nobilis* sample was collected from the Mediterranean Sea. The samples were cut along lines and directions of growth, perpendicularly to the surface of the studied shells, and then separately embedded in epoxy resin. The samples were ground and polished as the standard metallographic preparation route: mechanical polishing with silicon carbide papers 220 - 7000 grit followed by 1 μm and 0.25 μm diamond suspension and a final polishing step with colloidal silica suspension for 5 min using a Struers Tegramin-25 automatic polisher. The morphology and the surface characterization of fractured shells were studied by Leica DVM6 digital microscope. EBSD analyses were carried out using a FEI Versa 3D scanning electron microscope (SEM) equipped with EDAX Hikari CCD camera. Diffraction patterns were collected from samples under low vacuum (30 Pa of H_2O) at accelerating voltage (15 kV). The obtained EBSD data were analysed using the MTEX software [38].

Estimation of interfacial energy. According to the Gautam – Howe method, overlapping intensity *I* is a measure of the bonding strength at the phase boundary i.e. of matching the potential fields. Thus the higher the quantity *I*, the lower the energy of the interface treated as a disturbance [39]. In order to determine the distribution of total overlapping intensity *I*, in the Cartesian system $\hat{\boldsymbol{x}} \parallel [2\ \bar{1}\ \bar{1}\ 0]$, $\hat{\boldsymbol{y}} \parallel [0\ 1\ \bar{1}\ 0]$, $\hat{\boldsymbol{z}} \parallel (0\ 0\ 0\ 1)$, two calcite crystals are considered. One of them is fixed, while the other rotates around the axis $\boldsymbol{z}$ by an angle ω. The antisymmetric domain is investigated with an accuracy of 0.1°, thus $\omega \in \langle 0°,\ 60° \rangle$. Diffraction intensity I_i was assigned to each node in the reciprocal space using a structure factor $I_i = F_i \cdot F_i^*$[40, 41]. It is assumed that the intensity is distributed according to the Lorentzian function $s_i(r) = \frac{I_i \Gamma_i}{2\pi^2 r^2 (r^2 + \Gamma_i^2)}$, where Γ_i is the half of width at the half of the maximum. Γ_i constitutes the part of a sphere radius R_i bounding a reflection. With the appropriate relation R_i/Γ_i, the intensity contained in the sphere I_{ci} is almost all of the intensity I_i assigned to a given node: $I_{ci} = \int_0^{R_i} \int_0^{2\pi} \int_0^{\pi} s_i(r) r^2 \sin\varphi \mathrm{d}\varphi \mathrm{d}\theta \mathrm{d}r = \frac{2}{\pi} \arctan\left(\frac{R_i}{\Gamma_i}\right)$. It is assumed that $\Gamma_i = \frac{R_i}{12}$, then nearly 95% of the intensity I_i is taken into account. The distribution of diffraction intensities in the reciprocal space maps the potential field of a crystal. The introduction of a phase boundary significantly disturbs the continuity

of the field along a given family of planes if there is a considerable misfit between the systems of the planes in the neighbouring crystallites. Thus, it is assumed that the bonding along the most densely packed planes of calcite $(1\ 0\ \bar{1}\ 4)$ is broken when the mismatch amounts to 20%. As a result, using formulas derived in [42], radii of the individual spheres are obtained $R_i = \frac{0.1\, I_i}{d_1 I_1}$, d_1, I_1 are interplanar distance and intensity for the considered system of planes, respectively.

Identification of mechanical properties. Nano-indentation and nano-impact tests were carried out by means of NanoTest Vantage system with a diamond Berkovich three-sided pyramid indenter. Indentations were made parallel to the normal direction with a maximal load of 1.5 mN. In the two regions considered, grids of 2025 impressions 1 μm apart were performed, which allows the maps of hardness and reduced Young's modulus to be obtained. The average values of the mechanical characteristics for individual grains were determined on the basis of the frequency distribution of the contact stiffness *k*. The *k* means identify prisms with different orientation as well as the boundary zone filled with organic material. Assuming a certain standard deviation, we can distinguish points belonging to individual areas and as a result calculate average *H*, E_r that characterize them. The Nano Tests instruments open also the possibility to conduct an impact test [43]. The Berkovich indenter was used, which was moved away from the fixed specimen to obtain an accelerating force of 0.5 mN. The amplitude of the first rebound from the sample surface was measured, which gave information about the amount of energy dissipated in the material. Atomic force microscopy (AFM) measurements were determined by the Bruker Dimension ICON XR operating in PeakForce-QNM mode in air. Data analysis was performed by NanoScope Analysis software. At the last stage of research, the static compression test was carried out. A servo hydraulic test machine MTS 810, equipped with an additional 25 kN load cell and MTS clip gage extensometer was used. The specimens were cut from the shell using diamantine wire and had geometry of rectangular prism with an average cross-sectional dimension of 2 mm and an average height (thickness) of 1.2 mm. The samples were compressed in direction of the shell thickness under grip displacement control at a speed of 0.2 μm/s.

References

[1] Rodríguez-Navarro, A.B., Checa, A., Willinger, M.-G., Bolmaro, R., Bonarski, J. Crystallographic relationships in the crossed lamellar microstructure of the shell of the gastropod *Conus marmoreus*. *Acta Biomaterialia* **8**, 830–835 (2012).

[2] Volkmer, D., Harms, M., Gower, L., Ziegler A. Morphosynthesis of nacre-type laminated $CaCO_3$ thin films and coatings. *Angewandte Chemie International Edition* **44**, 639–644 (2005). doi:10.1002/anie.200461386.

[3] Finnemore, A., Cunha, P., Shean, T., Vignolini, S., Guldin, S., Oyen, M., Steiner U. Biomimetic layer-by-layer assembly of artificial nacre. *Nature Communications* **3**, 966, 1-6 (2012). doi:10.1038/ncomms1970.

[4] Xiao, Ch., Li, M., Wang, B., Liu, M.-F., Shao, Ch., Pan, H., Lu, Y., Xu, B.-B., Li, S., Zhan, D., Jiang, Y., Tang, R., Liu, X. Y., Cölfen H. Total morphosynthesis of biomimetic prismatic-type CaCO3 thin films. *Nature Communications* **8**, 1398 (2017). doi:10.1038/s41467-017-01719-6.

[5] Zhao, H., Yang, Z., Guo, L. Nacre-inspired composites with different macroscopic dimensions: strategies for improved mechanical performance and applications. *NPG Asia Materials* **10**, 1-22 (2018). doi: 10.1038/s41427-018-0009-6.

[6] Schenk, S., Zlotnikov, I., Pokroy, B., Gierlinger, N., Masic, A., Zaslansky, P., Fitch, A. N., Paris, O., Metzger, T. H., Cölfen, H., Fratzl, P., Aichmayer, B. Hierarchical calcite crystals with occlusions of a simple polyelectrolyte mimic complex biomineral structures. *Advanced Functional Materials* **22**, 4668-4676 (2012). doi:10.1002/adfm.201201158.

[7] Metzger, T.H., Politi, Y., Carbone, G., Bayerlein, B., Zlotnikov, I., Zolotoyabko, E., Fratzl, P. Nanostructure of biogenic calcite and its modification under annealing: study by high-resolution X-ray diffraction and nanoindentation. *Crystal Growth & Design* **14**, 5275–5282 (2014). doi:10.1021/cg501068e.

[8] García-March, J., García-Carrascosa, A., Cantero, A., Wang, Y.-G. Population structure, mortality and growth of *Pinna nobilis* Linnaeus, 1758 (Mollusca, Bivalvia) at different depths in Moraira bay (Alicante, western Mediterranean). *Marine Biology* **150**, 861 – 871 (2007).

[9] Harper, E.M., Checa, A.G., Tightly shut: Flexible valve margins and microstructural asymmetry in pterioid bivalves. *Marine Biology* **167**, 78 (2020). doi:10.1007/s00227-020-03693-y.

[10] Zavodnik, D., Hrs-Brenko, M., Legac, M., Synopsis on the fan shell *Pinna nobilis* L. in the eastern Adriatic Sea, In Boudouresque C.F. et al. (eds) *Les espèces marines à protèger en Méditerranée*. (Marseille: GIS Posidonie Publication, 1991).

[11] Dauphin, Y., Soluble organic oatrices of the calcitic prismatic shell layers of two pteriomorphid bivalves - *Pinna nobilis* and *Pinctada margaritifera*. *Journal of Biological Chemistry* **278** (17), 15168–15177 (2003). doi:10.1074/jbc.m204375200.

[12] Marin, F., Narayanappa, P., Motreuil, S. Acidic shell proteins of the Mediterranean fan mussel *Pinna nobilis*, In Müller, W.E.G. (ed.), *Molecular Biomineralization: Aquatic Organisms Forming Extraordinary Materials* (Springer, Heidelberg, Germany, 2011).

[13] Harper, E.M., Checa, A. Physiological versus biological control in bivalve calcite prisms: Comparison of euheterodonts and pteriomorphs. *The Biological Bulletin* **232** (1), 19–29 (2017). doi:10.1086/691382.

[14] Checa, A.G., Bonarski, J.T., Willinger, M.G., Faryna, M., Berent, K., Kania, B., González-Segura A., Pina, C. M., Pospiech, J., Morawiec, A. Crystallographic orientation inhomogeneity and crystal

splitting in biogenic calcite. *Journal of the Royal Society Interface* **10** (86), 20130425 (2013). doi:10.1098/rsif.2013.0425.

[15] Addadi, L., Politi, Y., Nudelman, F., Weiner, S. Biomineralization design strategies and mechanisms of mineral formation: operating at the edge of instability, In Novoa, J.J., Braga, D., Addadi, L. (eds) *Engineering of Crystalline Materials Properties: State of the Art in Modeling, Design and Applications* (Springer, Dordrecht, Netherlands 2007).

[16] Okumura, T., Suzuki, M., Nagasawa, H., Kogure, T. Characteristics of biogenic calcite in the prismatic layer of a pearl oyster, *Pinctada fucata*. *Micron* **41** (7), 821–826 (2010). doi:10.1016/j.micron.2010.05.004.

[17] Marin, F., Pokroy, B., Luquet, G., Layrolle, P., De Groot, K. Protein mapping of calcium carbonate biominerals by immunogold. *Biomaterials* **28** (14), 2368–2377 (2007). doi:10.1016/j.biomaterials.2007.01.029.

[18] Dauphin, Y., Zolotoyabko, E., Berner, A., Lakin, E., Rollion-Bard, C., Cuif, J.P., Fratzl, P., Breaking the long-standing morphological paradigm: Individual prisms in the pearl oyster shell grow perpendicular to the c-axis of calcite. *Journal of Structural Biology* **205**, 121–132 (2019). doi: 10.1016/j.jsb.2019.01.004.

[19] Dauphin, Y. Comparison of the soluble matrices of the calcitic prismatic layer of *Pinna nobilis* (Mollusca, Bivalvia, Pteriomorpha). *Comparative Biochemistry and Physiology Part A: Molecular & Integrative Physiology* **132** (3), 577–590 (2002). doi:10.1016/s1095-6433(02)00099-5.

[20] Marin, F., Luquet, G., Marie, B., Medakovic, D. Molluscan shell proteins: Primary structure, origin, and evolution. *Current Topics in Developmental Biology* **80**, 209–276 (2007). doi:10.1016/s0070-2153(07)80006-8.

[21] Checa, A.G., Esteban-Delgado, F. J., Ramírez-Rico, J., Rodríguez-Navarro, A. B. Crystallographic reorganization of the calcitic prismatic layer of oysters. *Journal of Structural Biology* **167**, 261–270 (2009). doi:10.1016/j.jsb.2009.06.009.

[22] Sommerdijk, N., Cusack, M. Crystals competing for space. *Nature Materials* **13**, 1078–1079 (2014). doi:10.1038/nmat4147.

[23] Bayerlein, B., Zaslansky, P., Dauphin, Y., Rack, A., Fratzl, P., Zlotnikov, I. Self-similar mesostructure evolution of the growing mollusc shell reminiscent of thermodynamically driven grain growth. *Nature Materials* **13**, 1102–1107 (2014). doi: 10.1038/nmat4110.

[24] Checa, A.G., Macías-Sánchez, E., Harper, E.M., Cartwright, J.H.E. Organic membranes determine the pattern of the columnar prismatic layer of mollusc shells. *Proc. R. Soc. B* **283**, 20160032 (2016). doi:10.1098/rspb.2016.0032.

[25] Dauphin, Y., Brunelle, A., Medjoubi, K., Somogyi, A., Cuif, J.-P. The prismatic layer of *Pinna:* A showcase of methodological problems and preconceived hypotheses. *Minerals* **8** (9), 365 (2018). doi:10.3390/min8090365.

[26] Jackson, P., Vincent, J. F. V., Turner, R. M. The mechanical design of nacre, *Proceedings of the Royal Society of London, Series B* **234**, 415–440 (1988). doi:10.1098/rspb.1988.0056.

[27] Barthelat, F., Espinosa, H. D. An experimental investigation of deformation and fracture of nacre–mother of pearl. *Experimental Mechanics* **47**, 311–324 (2007). doi:10.1007/s11340-007-9040-1.

[28] Rabiei, R., Dastjerdi, A. K., Barthelat, F. Interfacial fracture toughness of nacre, in Prorok, B. C., Korach, Ch. S., Lipke, E., Zavattieri, P., Barthelat, F., Grande-Allen, K. J., Lykofatitits, G., *Mechanics of Biological Systems and Materials, Volume 5: Proceedings of the 2012 Annual Conference on Experimental and Applied Mechanics* (Springer, London, 2013).

[29] Gim, J., Schnitzer, N., Otter, L.M., Cui, Y., Motreuil, S., Marin, F., Wolf, S. E., Jacob, D. E., Misra, A., Hovden, R. Nanoscale deformation mechanics reveal resilience in nacre of *Pinna nobilis* shell, *Nature Communications* **10**, 4822 (2019). doi:10.1038/s41467-019-12743-z.

[30] Taylor, J. D., Layman, M. The mechanical properties of bivalve (mollusca) shell structures. *Palaeontology* **15**, 73-87 (1972).

[31] Strąg, M., Maj, Ł., Bieda, M., Petrzak, P., Jarzębska, A., Gluch, J., Topal, E., Kutukova, K., Clauser, A., Heyn, W., Berent, K., Nalepka, K., Zschech, E., Checa, A. G., Sztwiertnia, K. Anisotropy of mechanical properties of *Pinctada margaritifera* mollusk shell. *Nanomaterials* **10**, 634 (2020). doi:10.3390/nano10040634.

[32] Kunitake, M. E., Mangano, L. M., Peloquin, J. M., Baker, Sh. P., Estroff L. A. Evaluation of strengthening mechanisms in calcite single crystals from mollusk shells. *Acta Biomaterialia* **9**, 5353–5359 (2013). doi:10.1016/j.actbio.2012.09.030.

[33] Böhm, F., Feldner, P., Merle, B., Wolf, S. E. Conical nanoindentation allows azimuthally independent hardness determination in geological and biogenic minerals. *Materials* **12** (10), 1630 (2019). doi:10.3390/ma12101630.

[34] Gautam, A.R.S., Howe, J.M. A method to predict the orientation relationship, interface planes and morphology between a crystalline precipitate and matrix. Part I, approach. *Philosophical Magazine* **91**, 3203-3227 (2011). doi: 10.1080/14786435.2011.573817.

[35] De Bresser, J.H.P., Spiers, C.J. Strength characteristics of the r, f, and c slip systems in calcite. *Tectonophysics* **272**, 1-23 (1997). doi: 10.1016/S0040-1951(96)00273-9.

[36] Bruno, M., Massaro, F. R, Pastero, L., Costa, E., Rubbo, M., Prencipe, M., Aquilano D. New estimates of the free energy of calcite/water interfaces for evaluating the equilibrium shape and nucleation mechanisms. *Crystal Growth & Design* **13**, 1170−1179 (2013). doi:10.1021/cg3015817.

[37] Hagan, J.T. Micromechanics of crack nucleation during indentations. *Journal of Materials Science* **14**, 2975–2980 (1979). doi: 10.1007/BF00611482.

[38] Bachmann, F. Hielscher, R., Schaeben, H. Texture analysis with MTEX - free and open source software toolbox. *Solid State Phenomena* **160**, 63-68 (2010). doi.org/10.4028/www.scientific.net/SSP.160.63.

[39] Nalepka K., Sztwiertnia K., Nalepka P. Preferred orientation relationships at the Cu/α-Al_2O_3 interface: Identification and theoretical explanation. *Acta Materialia* **104**, 156-165 (2016). doi: 10.1016/j.actamat.2015.11.014.

[40] Fultz, B., Howe, J. *Transmission Electron Microscopy and Diffractometry of Materials* (Springer, Berlin, 2001).

[41] Prince E. (Ed) *International Tables for Crystallography Vol. C*: *Mathematical, physical and chemical tables* (Wiley, New York, 2006).

[42] Beake, B.D., Goodes S.R. & Smith J.F. Micro-Impact Testing: A New Technique for Investigating Thin Film Toughness, Adhesion, Erosive Wear Resistance, and Dynamic Hardness. *Surface Engineering* **17**, 187-192 (2001). doi: 10.1179/026708401101517755.

Acknowledgements

The authors thank Mr Alan Krawczyk from Technolutions company for the possibility of performing microstructural analysis using a Leica DVM6 digital microscope. The work was supported by the Polish National Agency for Academic Exchange (grant PPI/APM/2018/1/00049/U/001) and the National

Science Center (grant UMO-2018/29/B/ST8/02200). AGC was funded by project CGL2017-85118-P of the Spanish Ministerio de Ciencia e Innovación.

Author contributions

K.N., A.Ch, K.Sz., K.B. proposed and supervised the project; M.S., Ł.M. prepared the samples; K.N., K.B., T.M., A.J.H., P.N. analysed the data and provided some experimental assistance; K.N., T.M., A.J.H. contributed to the analysis of data and mechanical measurements. K.B. performed the SEM/EBSD measurements; A. Sz. carried out the AFM measurements; KN performed calculations constituting the basis for the theoretical analysis of microstructure and mechanical properties. K.N., K.B. and A.Ch. collectively wrote the manuscript; All authors contributed to the discussion.

Competing interests: the authors declare no competing interests.